

Energetics of selective cleavage at acidic residues studied by time- and energy-resolved surface-induced dissociation in FT-ICR MS

Thomas H. Bailey^a, Julia Laskin^{b,*}, Jean H. Futrell^b

^a Department of Chemistry and Biochemistry, University of Delaware, Newark, DE 19716, USA

^b William R. Wiley Environmental Molecular Sciences Laboratory, Pacific Northwest National Laboratory, P.O. Box 999 (K8-96), Richland, WA 99352, USA

Received 1 May 2002; accepted 27 September 2002

Abstract

Surface-induced dissociation (SID) of four model peptides: LDIFSDF, LDIFSDFR, RLDIFSDF, and LEIFSEFR, was studied using a novel Fourier transform ion cyclotron resonance mass spectrometer (FT-ICR MS) specially equipped to perform SID experiments. The energetics and dynamics of selective cleavages at acidic residues were deduced by modeling the time- and energy-resolved fragmentation efficiency curves (TFECs) using an RRKM-based approach developed in our laboratory. RRKM modeling revealed that addition of a basic residue—arginine—to the C-terminus of a peptide has a very small effect on the dissociation threshold. However, the dynamics of dissociation is dramatically affected by the presence of arginine. The Arrhenius pre-exponential factor for dissociation of LDIFSDF is two orders of magnitude higher than the pre-exponential factor for dissociation of arginine-containing peptides. The difference in the pre-exponential factors is indicative of a complex rearrangement process associated with selective fragmentation. Molecular mechanics modeling of the four parent ions gives some qualitative insight into the differences in fragmentation mechanisms. (Int J Mass Spectrom 222 (2003) 313–327) © 2002 Elsevier Science B.V. All rights reserved.

Keywords: Surface-induced dissociation; RRKM modeling; Selective cleavage; Protonated peptides; Fragmentation energetics

1. Introduction

Electrospray ionization is an effective method for ionization of many biologically relevant molecules [1,2]. Additionally, surface-induced dissociation (SID) is not only an effective means for activation of large biological ions but also provides valuable peptide sequence information [3,4]. Physical and chemical processes occurring during collisions of low

energy (1–100 eV) polyatomic ions with different surfaces have been recently reviewed [5]. Self-assembled monolayers (SAMs) of fluorinated alkyl thiols on gold substrates are preferred targets for SID studies because of the reduced neutralization efficiency compared to metal surfaces and the relatively high efficiency of internal excitation that can be easily achieved. Following collision of a protonated parent ion with a SAM surface, a significant percentage (12–35%) of the parent ion's kinetic energy is converted into the internal energy [4]. This virtually instantaneous increase in

* Corresponding author. E-mail: julia.laskin@pnl.gov

the ion's internal energy results in fragmentation that, for the peptides investigated here, is well described by an RRKM-based statistical model.

Most of the SID instruments in use today are of the "tandem-in-space" variety. These instruments usually consist of a quadrupole for mass selection of the parent ion and incorporate quadrupole or TOF detectors for fragment ion mass analysis [6–10], providing good parent ion selection as well as efficient detection of fragment ions. However, because of the short time scales of these instruments (ca. 10 μ s) dissociation of complex polyatomic ions is associated with a substantial kinetic shift. The kinetic shift, defined as the amount of internal energy necessary for the ion to fragment on the time scale of the instrument [11], is quite large for complex peptide ions dissociating on a microsecond time scale. The high internal excitation required to observe fragmentation in these instruments results in efficient opening of a variety of dissociation channels, even at the lowest collision energies. Consequently, it is increasingly difficult to distinguish between the high- and the low-energy fragmentation pathways as the complexity of the precursor ion increases.

Coupling SID with a Fourier transform ion cyclotron resonance mass spectrometer (FT-ICR MS) provides the distinct advantages of long and variable reaction times (milliseconds to seconds), which both greatly reduces the kinetic shift and provides a means for investigating kinetic shifts phenomenologically. Reducing the kinetic shift results in shifting fragmentation efficiency curves to much lower collision energies than are observed in tandem in-space instruments. Moreover, studying ion fragmentation following impact with a surface in the FT-ICR MS enables both accessing the lowest energy channels at low collision energies and accessing separately higher-energy channels that open at higher internal excitation.

Surface-induced dissociation spectra of peptides are characterized by backbone cleavages resulting in formation of **b** and **y** type ions. A **b_n** ion is formed if the charge remains on the N-terminus, while a **y_n** ion is the result of the charge remaining on the C-terminus. The *n* refers to which peptide bond has been cleaved,

counting from the N-terminus for **b** ions and from the C-terminus for **y** ions [12,13]. These **b_n** and **y_n** type ions are extremely effective at assigning the relative positions of the amino acids within the peptide chain being studied.

Most SID spectra of peptides contain numerous **b_n** and **y_n** fragment ions, as well as fragment ions resulting from additional losses of H₂O, NH₃, CO and internal fragments. However, it has been demonstrated that peptides containing a highly basic amino acid, such as arginine or lysine, and aspartic or glutamic acid in the sequence fragment selectively at acidic residues [14–18]. A fragmentation spectrum resulting from selective cleavage of a peptide contains only a small number of fragment ions. These fragment ions are typically of only one type, either **b_n** or **y_n**, depending on which end of the peptide includes the basic residue.

Several groups have studied selective cleavages at acidic residues. Beauchamp and co-workers made some of the first observations of selective cleavages at aspartic acid in experiments involving collision-induced dissociation (CID) of sodiated peptides [19]. They pointed out that sodiated peptides fragmented via highly specific cleavages C-terminal to aspartic acid. They suggested a salt bridge mechanism in which the sodium ion stabilized the ion pair intermediate formed by transfer of a proton from the carboxylic acid side chain of aspartic acid to the adjacent amide nitrogen of the peptide bond. A similar mechanism was proposed by Gaskell and co-workers to rationalize selective cleavages of protonated peptides at acidic residues in the presence of arginine [16]. The interaction between the protonated guanidino group of the arginine with the carboxylic acid side chain of the aspartic acid residue results in deprotonation of the acidic side chain followed by the proton transfer to the amide nitrogen located C-terminal to the acidic residue. This results in a facile cleavage of the corresponding peptide bond.

Wysocki and co-workers found that selective cleavages occur in arginine-containing peptides when the number of ionizing protons does not exceed the number of basic residues [17]. They proposed a different mechanism of selective fragmentation that favors

remote cleavage at the acidic residues in which the ionizing proton resides on the highly basic arginine side chain and does not play an active role in the cleavage [17,18]. The protonated arginine side chain is solvated through an interaction with the closest carboxylic acid group, while selective cleavage occurs at the acidic residue remote from the protonated guanidino group. The cleavage is initiated by the acidic proton of the aspartic acid side chain interacting with the amide nitrogen of the C-side peptide bond.

Recent work by Gaskell and co-workers [20] has shown the utility of coupling selective cleavages to database searching in peptide mass mapping. Experiments involving CID of tryptic peptide fragments demonstrated that knowing the location of an aspartic acid residue within the tryptic fragment greatly reduces the number of tryptic fragments necessary for accurate protein identification via database searching. We infer that defining the mechanism(s), by which selective cleavages take place and the resulting ability to predict mass spectral characteristics will significantly improve computer-based techniques for peptide and protein identification.

In this study we present a detailed investigation of the energetics of selective cleavages at acidic residues by examining time- and energy-resolved fragmentation of four peptides that vary in the content and relative position of an arginine residue (LDIFSDF, LDIFSDFR, RLDIFSDF, LEIFSEFR). Fragmentation of these peptides has been studied recently using a variety of activation techniques [16,17]. Three of the peptides studied fragment via selective cleavages (LDIFSDFR, RLDIFSDF, and LEIFSEFR), while the fourth fragments totally non-selectively (LDIFSDF). All three of the peptides that fragment selectively contain an arginine (R) and either two aspartic acids (D) or two glutamic acids (E). The fourth peptide, LDIFSDF, contains two aspartic acid residues, but no arginine.

In this work we utilized an RRKM-based modeling approach developed in our laboratory [21,22] to extract the energetics and dynamics of peptide fragmentation from the time- and energy-resolved data. This approach has been previously applied to study fragmentation energetics of small alanine-containing

peptides [23,24]. Arrhenius pre-exponential factors extracted from the modeling indicate that parent ion decomposition via selective cleavages proceeds slower, by two orders of magnitude, than parent ion decomposition via non-selective cleavages. This is a result of the large negative entropy changes calculated for the arginine-containing peptides, indicating that selective cleavages take place only after complex rearrangements.

2. Experimental

Surface-induced dissociation experiments were conducted on a home-built 6T FT-ICR mass spectrometer. The instrument is equipped with a high-transmission electrospray source, consisting of an ion funnel interface [25] followed by three quadrupoles. The instrument is also fitted with a vacuum interlock assembly that allows the SID target to be positioned just inside the rear trapping plate of the ICR cell. Both the instrument and SID experiment have been detailed elsewhere [26] and will only be briefly outlined below.

The SAM surface was prepared on a single gold crystal (Monocrystals, Richmond Heights, OH) using a standard procedure. The target was cleaned in a UV cleaner (Model 135500, Boekel Industries Inc., Feasterville, PA) for 10 min and allowed to stand in a 1 mM ethanol solution of FC₁₂ (CF₃(CF₂)₉C₂H₄SH), for 24–36 h. The target was removed from the SAM solution and ultrasonically washed in ethanol for 10 min to remove extra layers. Immediately after washing, the SAM surface is positioned on the end of an insertion probe and is inserted into the ultra-high vacuum region of the FT-ICR, through a vacuum interlock at the rear of the instrument. The surface is positioned 1–2 mm inside of the rear trapping plate of the ICR cell. Once positioned, the surface is electrically connected to the rear trapping plate power supply. This ensures that the SAM surface and the rear trapping plate are at the same potential throughout the experiment.

Ions are electrosprayed, at atmospheric pressure, into the end of a heated stainless steel capillary tube. The ions travel through the capillary tube, into the

vacuum system, and into the entrance of the ion funnel. The ion funnel provides highly efficient ion transfer into the high vacuum region of the mass spectrometer. The first quadrupole, immediately following the ion funnel, collisionally cools the ions exiting the ion funnel. Upon exiting the first quadrupole, the parent ion of interest (singly protonated ions in all of the following experiments) is mass selected in the second quadrupole and accumulated in the third quadrupole for 0.3–0.8 s. The third (accumulation) quadrupole is held at an elevated pressure (2×10^{-3} Torr) for collisional relaxation of stored ions. Collisional relaxation is necessary to insure efficient thermalization of the parent ion population.

After accumulation, the ions are extracted from the third quadrupole with an extraction pulse 250 μ s wide (ion accumulation and ejection are controlled by applying the necessary voltages to apertures positioned on either side of Quadrupole three). Following ion ejection, a time-of-flight (TOF) delay allows the ions time to fly through the transfer optics to the ICR cell where they collide with the surface. The TOF delay is typically 80–140 μ s, depending on the parent ion mass. Scattered ions are captured by raising the potentials on the front and rear trapping plates of the ICR cell by 10–15 V. Time-resolved mass spectra were acquired by varying the delay between the gated trapping and the excitation/detection event (the reaction delay). Typically, the reaction delay was varied from 1.0 ms to 1.0 s. Immediately following the reaction delay, ions were excited by a broadband chirp and detected.

The collision energy is defined by the difference in the potential applied to the accumulation quadrupole and the potential applied to the rear trapping plate and the SID target. The ICR cell can be offset above or below ground by as much as ± 150 V. Lowering the ICR cell below ground, while keeping the potential on the third quadrupole fixed, increases collision energy for positive ions. Because ion energy is changed within the constant high magnetic field region of the ICR we anticipated and have shown that the ion transmission characteristics of the instrument remain the same at all collision energies. Consequently, parent ion currents

and ion trajectories are constant and independent of collision energy [26].

Experimental control is accomplished with the MIDAS data station [27]. MIDAS is used to control the voltages and timing of the source and transfer optics, as well as the excite/detect events in the ICR cell. An automated script was written to allow for unattended acquisition of kinetic data. The script was used to vary the reaction delay and collision energy of the experiment. Reaction delays of 1, 10, 50 ms, 0.1, 0.3, and 1 s were studied. Typical experiments involved changing the collision energy across a relatively wide range (5–60 eV). The automated script allowed for acquisition of SID spectra across the entire range of collision energies, in 1 eV increments, at each of the six reaction delays. Time-dependent fragmentation efficiency curves (TFECs) were constructed from experimental mass spectra by plotting the relative intensity of the precursor ion as a function of collision energy for each reaction delay.¹

Samples of LDIFSDF, LDIFSDFR, RLDIFSDF were provided by Prof. V.H. Wysocki; LEIFSEFR was purchased from Pepton Inc. (Taejon, South Korea) and used as received. All samples were dissolved in a 70:30 (v/v) methanol:water solution with 1% acetic acid. A syringe pump (Cole Parmer, Vernon Hills, IL) was used for direct infusion of the electrospray samples at flow rates ranging from 20 to 50 μ L/h.

2.1. RRKM modeling

The TFECs were modeled using an RRKM-based approach developed by our group [21–24]. Energy-dependent microcanonical rate constants for the total decomposition of the precursor ion, $k(E)$, were calculated using RRKM/QET. Relative abundance of the parent and the fragment ions as a function of the internal energy of the parent ion and the experimental

¹ It should be noted that this definition of the FEC is different from the definition used in some other SID studies, where the FEC is constructed by plotting the relative yield of all fragment ions. The current definition allows constructing the fragmentation efficiency curve for each ion in the spectrum (including the precursor ion) in the same way.

observation time (t_r), $F(E, t_r)$, was calculated taking into account radiative cooling of the excited ion. The energy deposition function was described by the following analytical expression:

$$P(E, E_{\text{coll}}) = \frac{1}{C}(E - \Delta)^l \exp\left(-\frac{E - \Delta}{f(E_{\text{coll}})}\right) \quad (1)$$

where $C = \Gamma(l + 1)[f(E_{\text{coll}})]^{l+1}$ is a normalization factor, l and Δ are parameters, and $f(E_{\text{coll}})$ has the form:

$$f(E_{\text{coll}}) = A_2 E_{\text{coll}}^2 + A_1 E_{\text{coll}} + A_0 \quad (2)$$

where A_0 , A_1 and A_2 are parameters, and E_{coll} is the collision energy.

Finally, the normalized signal intensity for a particular reaction channel is given by the equation:

$$I_i(E_{\text{coll}}) = \int_0^\infty F_i(E, t) P(E, E_{\text{coll}}) dE \quad (3)$$

Collision energy-resolved fragmentation efficiency curves at different reaction times (TFECs) were constructed using the above procedure and compared to experimental data. The energy deposition function was kept the same for all reaction times. The fitting parameters were varied until the best fit to experimental fragmentation efficiency curves was obtained. The fitting parameters included critical energies and activation entropies of the major reaction channels and parameters characterizing the energy deposition function (Eqs. (1) and (2)). The uniqueness of the fits was confirmed using sensitivity analysis described elsewhere [22,23].

Vibrational frequencies of precursor ions were obtained from the frequency model given by Christie and co-workers [28]. Vibrational frequencies for the transition state were estimated by removing one C–N stretch (reaction coordinate) from the parent ion frequencies as well as varying 15 frequencies in the range of 300–1500 cm^{-1} to obtain the best fit with experimental data.

2.2. Molecular mechanics modeling

Molecular mechanics modeling of parent ion conformations was done using the Discover module of the

Insight II software suite (Biosym Technologies, San Diego, CA). The peptides were constructed using the amino acid library contained in the Biopolymer module. Both the N- and C-terminus of the peptide were capped with hydrogens and left neutral. The ionizing proton was then placed at the most basic sight (the N-terminus for LDIFSDF, and the arginine side chain for LDIFSDFR, RLDIFSDF, and LEIFSEFR). Using the Discover module the structures were subjected to a steepest descent minimization for 1500 iterations using the CFF91 force field. After minimization, the optimized structures were repeatedly annealed at 400 K for 1500 cycles. The resulting annealed structures were again minimized and the resulting minimized structure annealed again. The process was repeated until a local minimum was achieved and the intramolecular interactions could be observed. Intramolecular hydrogen bonding was observed by turning on the hydrogen bonding feature of the program, using the default parameters, during the minimization and annealing (dynamics) experiments. All other parameters for the minimization and annealing were left at their default values. Approximately 15 structures obtained by repeated annealing/optimization were compared for each of the four peptides.

3. Results and discussion

3.1. Dissociation pathways

Surface-induced dissociation spectra for RLDIFSDF, LDIFSDFR, LEIFSEFR, and LDIFSDF are shown in Fig. 1. The spectra were acquired at a reaction delay of 1.0 s and at collision energies of 39.5, 39.5, 31.5, and 21.5 eV, respectively. In agreement with previous studies [16,17] SID spectra for the three arginine-containing peptides (RLDIFSDF, LDIFSDFR, LEIFSEFR) are clearly dominated by specific cleavages C-terminal to either the aspartic acid (D) or glutamic acid (E) residues, depending on the peptide, while LDIFSDF is not.

The spectrum of RLDIFSDF is dominated by the \mathbf{b}_3 and \mathbf{b}_7 ions resulting from selective cleavages at

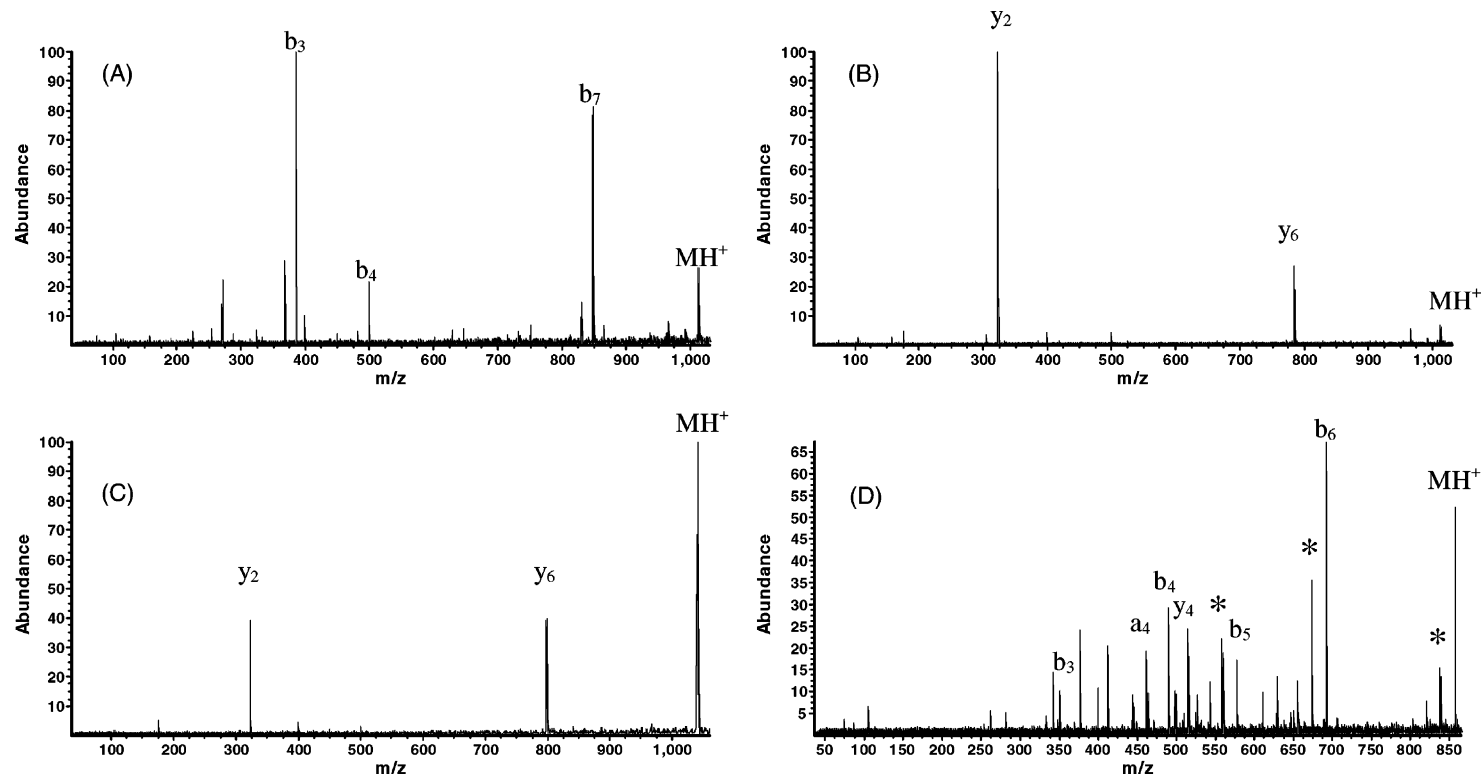


Fig. 1. Surface-induced dissociation spectra for: (A) RLDIFSDF, 39.5 eV collision; (B) LDIFSDFR, 39.5 eV collision; (C) LEIFSEFR, 31.5 eV collision; (D) LDIFSDF, 21.5 eV collision (* indicates a loss of water).

two aspartic acid residues (D) located in positions 3 and 7. A small amount of the \mathbf{b}_4 ion originating from a non-selective cleavage is observed in the mass spectrum. As expected, because of the relative position of the arginine residue, no \mathbf{y} -type ions are observed. Since arginine is the most basic residue in the peptide sequence it sequesters the proton during or immediately following electrospray ionization. After cleavage C-terminal to the aspartic acid (D) and glutamic acid (E) residues, the proton remains on the basic arginine residue as demonstrated by dominant \mathbf{b}_3 and \mathbf{b}_7 ions in the spectra.

Specific cleavages C-terminal to both aspartic acid (D) and glutamic acid (E) residues are also observed for the peptides LDIFSDFR and LEIFSEFR, respectively. Spectra from both peptides are dominated by \mathbf{y}_2 and \mathbf{y}_6 fragment ions. Highly basic arginine sequesters the proton and cleavage occurs C-terminal to both the aspartic acid (D) and glutamic acid (E) residues. As in the case of the RLDIFSDF, following cleavage the proton remains on the arginine residue. However, since the relative position of the arginine residue has moved to the C-terminus of the peptide, \mathbf{y} -type ions rather than \mathbf{b} -type ions are formed.

In the case of LDIFSDF, there is no highly basic amino acid to attract the ionizing proton. Therefore, the proton most likely resides on the N-terminus. Al-

though the \mathbf{b}_6 ion (resulting from cleavage C-terminal to the D residue in position 6) is the most abundant ion in the spectrum, many other fragment ions are observed in the SID spectrum indicating that LDIFSDF does not undergo specific cleavages.

Collision energy-resolved studies demonstrate that arginine-containing peptides fragment exclusively via selective cleavages at low collision energies. This confirms that these selective cleavages are the lowest-energy dissociation pathways. Fig. 2 shows fragmentation efficiency curves (FECs) obtained at a reaction delay of 1 ms for fragment ions resulting from selective cleavages at the acidic residues. The short time scale minimizes secondary fragmentation resulting from non-specific cleavages and/or consecutive dissociation of primary fragments. Arrows indicate the collision energy at which the overall intensity of other reaction channels (non-specific cleavages and consecutive fragmentation) rises above 10%. Interestingly, fragmentation efficiency curves for both fragments originating from selective cleavages overlap at low energies, indicating similar energetic requirements for both low-energy reaction channels. However, for LDIFSDFR and LEIFSEFR dissociation at the acidic residue remote from the arginine residue is somewhat slower than dissociation at the acidic residue located closest to arginine.

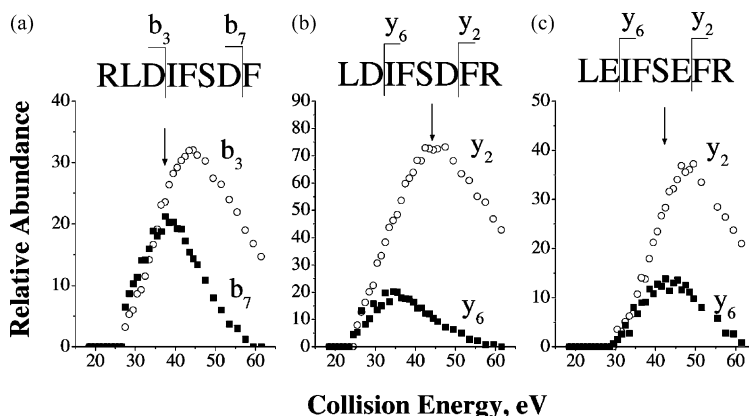


Fig. 2. Collision energy-resolved fragmentation efficiency curves for fragments originating from selective cleavages at two acidic residues for: (a) RLDIFSDF; (b) LDIFSDFR; (c) LEIFSEFR acquired at reaction time of 1 ms. The arrow represent the collision energy, at which dissociation through other pathways (non-selective cleavages and consecutive fragmentation of primary fragments) exceeds 10%.

This results in more extensive fragmentation at the acidic residue closest to arginine (y_2 fragment for both LDIFSDFR and LEIFSEFR) at all collision energies. It should be noted that in the case of RLDIFSDF, the essentially equal intensities of b_3 and b_7 ions are observed at low collision energies. Evidently a different secondary structure of this peptide is obtained than for peptides with arginine on the C-terminus.

Two different mechanisms for selective cleavages at acidic amino acid residues when arginine is present in the peptide sequence have been previously proposed. Summerfield et al. [16] suggested that interaction between the protonated guanidino group of arginine residue with the carboxyl group of the acidic residue results in the deprotonation of the acidic side chain and proton transfer to the amide nitrogen C-terminal to the acidic residue. The resulting structure is stabilized via a strong electrostatic interaction between the protonated guanidino group and deprotonated carboxylic group. Proton transfer weakens the adjacent amide bond and results in a facile fragmentation C-terminal to the acidic residue.

Wysocki and co-workers proposed a mechanism according to which interaction between the acidic and basic side chains results in charge solvation, while fragmentation preferentially occurs at acidic residues not involved in charge solvation [17]. This mechanism explains their observation that doubly protonated RLDIFSDFR displayed a selective cleavage only at the aspartic acid in position 7 (no cleavage at the third residue) resulting in the formation of the b_7/y_2 complementary pair of fragments. The charge-remote mechanism also accounts for the observed selective cleavages at acidic residues in fixed-charge derivatives of peptides containing aspartic acid [29]. In this case molecular ions of derivatized peptides are not protonated. However, even in the absence of a proton, selective cleavages occur at peptide bonds C-terminal to aspartic acid residues. These results are in qualitative agreement with observations made by Beauchamp and co-workers on selective fragmentation of sodiated peptides containing acidic residues [19], although the mechanistic explanation presented in the latter

study followed the previously discussed salt-bridge mechanism.

Our results for the fragmentation of LDIFSDFR and LEIFSEFR are in a good agreement with the charge-directed mechanism proposed by Summerfield et al. [16]. Specifically, dissociation at the aspartic or glutamic acid located closest to the arginine residue is somewhat faster than dissociation at the remote acidic residue. This suggests that the arginine residue is directly involved in dissociation process, providing a stronger interaction of the protonated guanidino group with the closest acidic side chain and initiating a faster cleavage at the amide bond adjacent to that side chain. However, the dissociation pattern of RLDIFSDF can be rationalized as a combination of the “salt-bridge” and the “remote” mechanisms. Fig. 2a indicates that the formation of the b_7 ion (cleavage remote from arginine) has a slightly lower threshold than the formation of the b_3 ion (cleavage close to the arginine residue). The latter channel is entropically favored and rises faster with collision energy. Competition of these two factors results in nearly equal production of b_3 and b_7 fragment ions at low collision energies.

3.2. Molecular mechanics modeling

Molecular mechanics modeling was done on all four peptides using the Insight II software suite to gain a better understanding of possible fragmentation mechanisms. Although not exhaustive, the search for minimum energy structures revealed several interesting trends described below. For example, we found that the non-arginine-containing peptide, LDIFSDF, has a very different conformation than the three arginine-containing peptides, LDIFSDFR, RLDIFSDF, and LEIFSEFR. The most obvious difference is the position of the ionizing proton. For LDIFSDF, the ionizing proton resides on the N-terminus, the most basic site for this peptide. In the three arginine-containing peptides the imine nitrogen of the guanidino group on the arginine side chain is the most basic site and is the site of protonation, rather than the N-terminus. In all four peptides the hydrogen atom on the carboxylic acid side chain of the aspartic acid

(D) and glutamic acid (E) residues is H-bonded to the nitrogen of the peptide bond immediately C-terminal to the acidic residue. This H-bonding results in the formation of a stable ring structure and rationalizes cleavages C-terminal to the aspartic and glutamic acids. However, this does not explain the dominance of selective cleavages when arginine is present in conjunction with the aspartic and glutamic acid residues in the peptides.

As stated above, the ionizing proton resides on either the N-terminus in LDIFSDF or on the arginine side chain in the three arginine-containing peptides. In the case of the three arginine-containing peptides, molecular mechanics modeling shows a strong tendency for the peptide chain to be wrapped around the basic side chain of the arginine residue. This results in extensive H-bonding between the basic arginine side chain and the side chains of the other amino acid residues, as well as significant H-bonding to the peptide backbone itself. In most of the optimized structures H-bonding interactions are observed between the acidic aspartic acid and glutamic acid residues and the basic side chain of the arginine residue. Interactions are also observed between the arginine side chain and the peptide bonds immediately N- and C-terminal to both the aspartic and glutamic acid residues. It is likely that this extensive H-bonding of the basic arginine side chain to the peptide bond, C-terminal to the aspartic and glutamic acid residues, as well as the H-bonding of the same peptide bond to the acidic side chains of the aspartic and glutamic acid residues, facilitates deprotonation of the acidic side chain followed by formation of a salt-bridge intermediate as suggested previously [16]. It should be emphasized that we do not suggest a proton transfer from the protonated guanidino group to the site of cleavage but rather infer that the proximity of the charge manifested by the presence of the hydrogen bonding between the basic side chain and the peptide bond being cleaved assists fragmentation.

More extensive solvation of the arginine side chain occurs when the arginine is located at the N-terminus of the peptide rather than the C-terminus, as in the case of RLDIFSDF. By positioning the arginine on

the N-terminus the protonated guanidino group of the arginine appears to have easier access to both acidic residues in the peptide. This explains the essentially equal intensities of the **b**₃ and **b**₇ ions at low collision energies (Fig. 2a). In contrast, molecular mechanics modeling of LDIFSDFR and LEIFSEFR indicates that preferential interaction occurs between the C-terminal arginine and the acidic residue in position 6 facilitating cleavage at D6 and E6 for LDIFSDFR and LEIFSEFR, respectively. In fact, all conformations in which the protonated guanidino grouping these peptides interacted with both acidic side chains after repeated heating and minimization steps converged to a family of structures with only one interaction with the closest acidic residue.

For LDIFSDF significant interaction between the carboxylic acid side chains and the nitrogen of the C-side peptide bond is present. This H-bonding facilitates breaking the peptide bond, to give the large **b**₆ ion observed in the LDIFSDF SID spectra. However, the lack of additional interactions with the highly basic arginine side chain results in formation of not only **b**₆ ions but also other fragments. The abundant **b**₆ ion in SID spectra of LDIFSDF can also result from a propensity observed previously in many studies of singly protonated peptides to lose the last amino acid residue. Further no large **b**₂ ion is observed from peptide bond cleavage C-terminal to the aspartic acid (D) residue in position 2. Selective cleavages are not observed in LDIFSDF since peptide bonds C-terminal to the aspartic and glutamic acids are not as destabilized as in the case of the arginine-containing peptides. This presumably reflects interactions of the peptide bond in question with the basic side chain of an arginine residue. Further work is required to define the interaction or interactions responsible for observed selective cleavages.

3.3. Collision energy-resolved fragmentation efficiency curves (FECs)

Fragmentation efficiency curves (FECs) for the four peptides obtained using a 1 s reaction delay are shown in Fig. 3. The FEC represents a plot of the relative

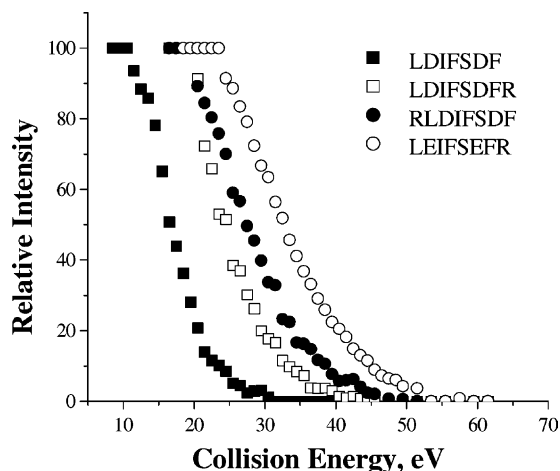


Fig. 3. Fragmentation efficiency curves (FECs) for LDIFSDF (filled squares), LDIFSDFR (open squares), RLDIFSDF (filled circles), and LEIFSEFR (open circles) at a reaction delay of 1.0 s.

intensity of the precursor ion as a function of collision energy. If the efficiency of kinetic-to-internal energy transfer ($T \rightarrow V$ transfer) is known, qualitative information on the relative stability of different peptide ions can be obtained based on the relative position of corresponding FECs. Our studies on the fragmentation of small alanine-containing peptides indicated that the efficiency of $T \rightarrow V$ transfer decreases monotonically with increasing peptide size for small peptides [30]. For larger peptides containing five amino acid residues very slow dependence of the $T \rightarrow V$ transfer efficiency on the peptide size was found. It can therefore be assumed that for the eight to nine residue peptides examined in this study the percent of energy transfer exhibits very slow dependence (if any) on peptide size. It follows that the relative stability of these peptides is directly reflected in the relative position of their FECs.

LDIFSDF is, by far, the easiest peptide to fragment of the four molecules studied. Its $E_{50\%}$ value is 8.6 eV lower than the next peptide in the order of increasing stability (LDIFSDFR) and 16.8 eV lower than the most stable peptide studied (LEIFSEFR). The three arginine-containing peptides are all more stable than the non-arginine-containing peptide and require more energy to reach the point of 50% fragmentation.

The $E_{50\%}$ data for LDIFSDFR and RLDIFSDF indicate that the RLDIFSDF is slightly more stable than the LDIFSDFR peptide. LEIFSEFR is the most stable of the four peptides studied, having an $E_{50\%}$ almost 8 eV higher than LDIFSDFR. This indicates that specific cleavages involving the glutamic acid residues of LEIFSEFR are energetically less favorable than selective cleavages involving the aspartic acid residues of LDIFSDFR, which is in good agreement with literature data [16,17].

LDIFSDFR is the same size as RLDIFSDF and has the same number of degrees of freedom. Both peptides contain two D residues and fragment via selective cleavages, yet their $E_{50\%}$ values differ by approximately 3 eV (24.6 and 27.4 eV, respectively). It follows that dissociation of the peptide with C-terminal arginine is energetically more favorable than dissociation of the peptide with arginine located at the N-terminus.

3.4. Time-resolved fragmentation efficiency curves (TFECs)

TFECs were acquired by varying the delay between trapping and excitation of the scattered ions (reaction delay). Fig. 4 shows TFECs for LDIFSDFR at the

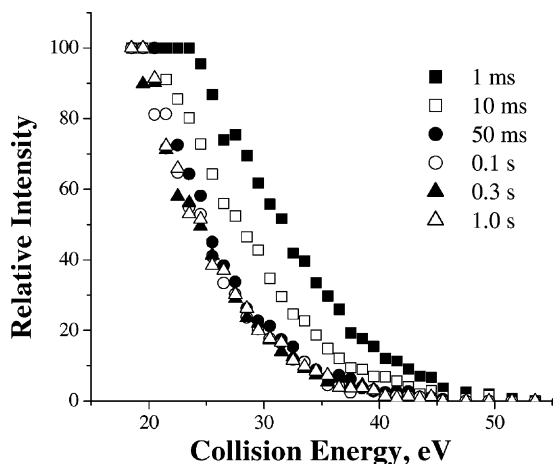


Fig. 4. Time-resolved fragmentation efficiency curves for LDIFSDFR at reaction delays of 1 ms (filled squares), 10 ms (open squares), 50 ms (filled circles), 0.1 s (open circles), 0.3 s (filled triangles), and 1 s (open triangles).

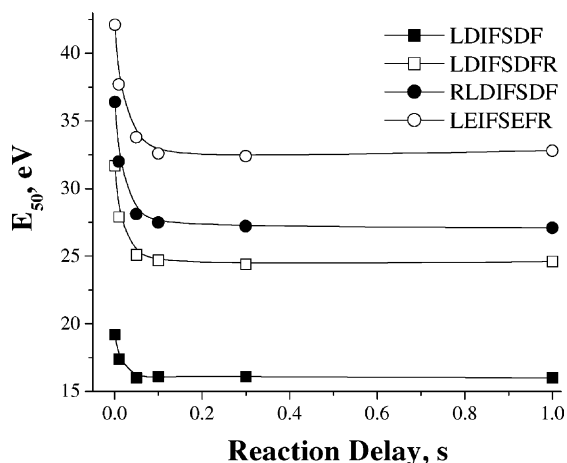


Fig. 5. Time dependence of the collision energy required to observe 50% fragmentation of the precursor ion ($E_{50\%}$).

six reaction times studied (1, 10, 50 ms, 0.1, 0.3, and 1 s). The energy required for fragmentation increases as the reaction delay decreases rather significantly at short times and becomes essentially invariant at longer times. This dependence is a direct result of the kinetic shift. To observe fragmentation on the shortest time scale (1 ms), the ion requires much greater internal energy relative to fragmentation occurring on the 1 s time scale. An increase in collision energy is required to achieve this increase in internal energy. In the case of LDIFSDFR, decreasing the reaction delay from 1 s to 1 ms results in a 7.1 eV increase in collision energy required to reach the point at which 50% of the parent ion has disappeared ($E_{50\%}$). It is noted that changing the time scale for fragmentation only affected the energies at which fragmentation was observed and had no effect on the types of fragment ions observed in the spectra.

Time dependence of the values of $E_{50\%}$ is summarized in Fig. 5. $E_{50\%}$ decreases dramatically as a function of reaction time at relatively short times and levels off at reaction times exceeding 0.1 s. The leveling off is associated with the competition between dissociation and radiative cooling of excited precursor ions. For radiative cooling to compete efficiently with dissociation on this time scale, the radiative rate for

all peptides should be of the order of 10 s^{-1} . Clearly, the slower the dissociation the more dramatic decrease in $E_{50\%}$ is observed as a function of reaction time. Shifts in the $E_{50\%}$, of 3.2, 7.1, 9.4, and 9.3 eV for LDIFSDF, LDIFSDFR, RLDIFSDF, and LEIFSEFR, respectively, were observed by changing the reaction delay from 1 ms to 1 s.

3.5. Modeling of experimental data

RRKM modeling of the experimental data provides quantitative values for dissociation threshold energies and decomposition rates and further rationalizes the trends observed in the experimental data. The TFECs for each of the four peptides were modeled using the RRKM-based approach briefly outlined above. The result of the modeling for LDIFSDFR is shown in Fig. 6. The points on the plot represent the experimental data, while the modeling results are represented by the lines. Fits of similar quality were obtained for other systems (results not shown).

Dissociation rate constants and modeling parameters for all four peptides are summarized in Fig. 7 and Table 1. The results of the modeling are in excellent

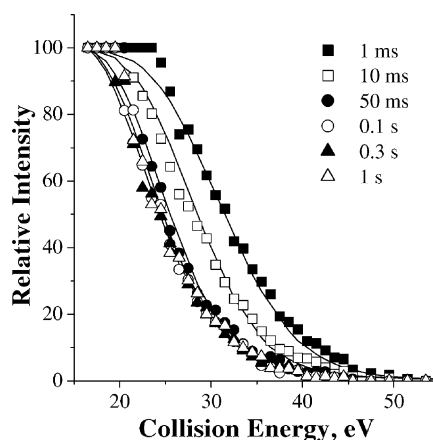


Fig. 6. RRKM modeling results fit to time-resolved fragmentation efficiency curves for LDIFSDFR. The modeling output is represented by the lines while the points represent the experiment TFECs for reaction delays of 1 ms (filled squares), 10 ms (open squares), 50 ms (filled circles), 0.1 s (open circles), 0.3 s (filled triangles), and 1 s (open triangles).

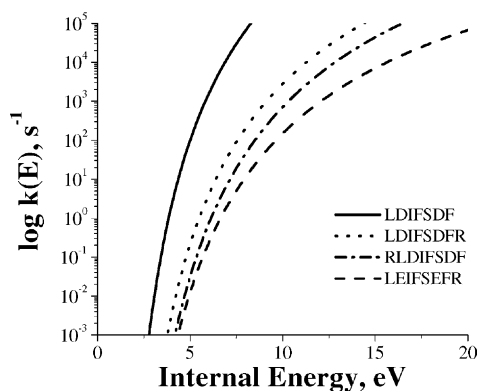


Fig. 7. Microcanonical rate-energy dependencies for LDIFSDF (solid line), RLDIFSDF (dash-dot line), LDIFSDFR (dotted line), and LEIFSEFR (dashed line).

agreement with the experimental data in terms of relative stability of the peptides. The threshold energies, E_0 , calculated from the RRKM modeling follow the same trends as the $E_{50\%}$ values observed experimentally with LDIFSDF being the least stable of the four peptides and LEIFSEFR being the most stable. It is interesting to note that addition of an arginine residue to the C-terminus of LDIFSDF results in a very small increase in the dissociation threshold (0.04 eV). The substantially faster dissociation of LDIFSDF, compared to dissociation of the arginine-containing peptides, mainly results from entropic effects that will be discussed later. The relative position of the arginine residue in the peptide sequence has a small but measurable effect on dissociation rates. Dissociation threshold for LDIFSDFR is 0.07 eV lower than disso-

ciation threshold for the peptide with the N-terminal arginine (RLDIFSDF). Replacing aspartic acid (D) with glutamic acid residue (E) results in a 0.09 eV increase in dissociation threshold, which is correlated to the difference in acidities of the corresponding side chains. Consequently, dissociation of LEIFSEFR is about 10 times slower than dissociation of LDIFSDFR (see Fig. 7).

The higher dissociation threshold observed for RLDIFSDF as compared to LDIFSDFR provides further support in favor of the “salt-bridge” (or charge-directed) mechanism discussed earlier. If arginine played the role of a charge holder with the cleavage initiated by acidic hydrogen of the aspartic acid remote from the site of protonation one would expect to obtain the same energetics and dynamics of fragmentation of these two peptides. In fact, arginine located at the C-terminus should be a better “charge holder” because it can interact with the C-terminus of the peptide and thereby stabilize the charge more efficiently than arginine in the N-terminal position. This implies that according to the charge-remote mechanism the dissociation threshold for RLDIFSDF should be the same or lower than the dissociation threshold for LDIFSDFR, which does not agree with our results.

It is remarkable that the differences in threshold energies (1.20, 1.24, 1.31, and 1.33 eV, for LDIFSDF, LDIFSDFR, RLDIFSDF, and LEIFSEFR, respectively) are so small in comparison with the differences in experimental values of $E_{50\%}$ (16.1, 24.6, 27.3, and 32.6 eV for LDIFSDF, LDIFSDFR, RLDIFSDF, and LEIFSEFR, respectively). The 0.07 eV

Table 1

Results of the RRKM modeling of the experimental time-dependent fragmentation efficiency curves

	LDIFSDF	LDIFSDFR	RLDIFSDF	LEIFSEFR
E_0 (eV)	1.20	1.24	1.31	1.33
ΔS^\ddagger (e.u.*)	-0.4	-7.9	-8.6	-12.5
A (s^{-1})	2.1E+13	4.8E+11	3.3E+11	4.6E+10
$T \rightarrow V$ transfer (%)	21.5	19.8	20.1	20.2
$E(k=1)$ (eV)	3.8	5.4	6.1	6.6

E_0 is the threshold energy, ΔS^\ddagger the entropy change for the transition state, A the pre-exponential factor, $T \rightarrow V$ transfer (%) the percentage of the ion's kinetic energy converted to internal energy upon collision, and E is the amount of internal energy required to cause fragmentation at a rate of $1 s^{-1}$.

* e.u. = cal/mol K.

difference in the threshold energy for LDIFSDFR and RLDIFSDF is translated into the 2.7 eV difference in $E_{50\%}$. This “amplification” of quite subtle variations in threshold energies results from a combination of two effects. First, there is a very substantial kinetic shift for dissociation of ions of this size even on a long time scale of the FT-ICR experiment. Internal energies required for dissociation rate constants of 1 s^{-1} , $E(k = 1)$, are listed in Table 1. The difference in internal energies required for dissociation of LDIFSDFR and RLDIFSDF is 0.7 eV. The second factor leading to the “amplification” is the efficiency of the kinetic-to-internal energy transfer. Average values of $T \rightarrow V$ transfer are close to 20% for all peptides. It follows that the difference in SID collision energies required observing fragmentation is about five times larger than the difference in the corresponding internal energies. This makes surface-induced dissociation in FT-ICR an extremely sensitive investigative tool for establishing small differences in fragmentation energetics and dynamics of large peptide ions.

Dissociation of all peptides is characterized by large negative activation entropy. However, dissociation of LDIFSDF is kinetically favored compared to dissociation of all arginine-containing peptides. The calculated Arrhenius pre-exponential factor for LDIFSDF is $2.1 \times 10^{13} \text{ s}^{-1}$. This value is two orders of magnitude higher than the pre-exponential factors calculated for the three arginine-containing peptides (4.8×10^{11} , 3.3×10^{11} , and $4.6 \times 10^{10} \text{ s}^{-1}$, for LDIFSDFR, RLDIFSDF, and LEIFSEFR, respectively). As a result, the rate of decomposition of LDIFSDF rises much faster with internal energy than the rate of decomposition of the arginine-containing peptides (see Fig. 7).

Replacing aspartic with glutamic acid results in lowering the pre-exponential factor by an order of magnitude. As a result, the microcanonical rate constant rises slower for LEIFSEFR than for the other two arginine-containing peptides. Clearly, the rate-energy dependencies for LDIFSDFR and LEIFSEFR diverge significantly at high internal energies required to obtain a rate constant of 10^5 s^{-1} , characteristic of tandem-in-space instruments. As a result, LEIFSEFR is characterized by a much larger kinetic shift on a

microsecond time scale than its analogs containing the aspartic acid residue. This suggests that selective cleavages in peptides containing glutamic acid residue are less likely to be observed on a microsecond time scale in the presence of other competing pathways that are expected to open up at high enough internal energies. This result is in agreement with the finding that selective cleavages at glutamic acid are observed only in trapping instruments sampling long reaction times [14,15].

The activation entropy for LDIFSDF differs from the activation entropies for the three arginine-containing peptides by approximately 8 e.u. (-0.4 , -7.9 , -8.6 , and -12.5 e.u. for LDIFSDF, LDIFSDFR, RLDIFSDF, and LEIFSEFR, respectively). Large negative entropy changes, and therefore low pre-exponential factors, may be a “signature” characteristic for complex rearrangement processes in peptides. This process can be associated either with a complex rearrangement, or constrained by a requirement for a very specific configuration to be reached in the transition state. The latter situation applies when only one conformation, or a small number of conformations, will result in the specific cleavage.

4. Conclusions

FT-ICR mass spectrometry is very well suited for time and energy-resolved SID studies. The long time scale of the FT-ICR instrument (milliseconds to seconds) results in decreased kinetic shifts for large molecules as compared to typical tandem-in-space SID instruments ($10 \mu\text{s}$ time scale). Varying the reaction delay between collision of the parent ion with the surface and fragment ion detection enables the construction of TFECs. From these TFECs qualitative observations could be made about the relative stabilities of the peptides studied, as well as the relative kinetics for the decomposition of the precursor ions.

We have demonstrated very efficient amplification of the small differences in threshold energies in our collision energy-resolved experiments. This makes FT-ICR SID an extremely sensitive tool for probing

small differences in dissociation thresholds of large molecules. The amplification results from the kinetic shift, which is observed for large peptides even on a long time scale of FT-ICR experiments, and the fact that only a fraction of the collision energy is converted into internal excitation of precursor ions. We have also shown that ion excitation by impact with a surface in combination with FT-ICR detection is an efficient means for studying both high- and low-energy fragmentation pathways, which are easily distinguished by their appearance energies.

In agreement with previous studies [14–17] we found that LDIFSDFR, RLDIFSDF, and LEIFSEFR fragmented via selective cleavages C-terminal to the aspartic and glutamic acid residues, while SID spectra for LDIFSDF were characterized by non-selective cleavages. The energetics and dynamics of selective and non-selective dissociation were determined using RRKM modeling of TFECs. We found that addition of a basic residue to peptides containing aspartic acid results in a very small increase in dissociation threshold, while the dynamics of dissociation is affected dramatically. The Arrhenius pre-exponential factor for dissociation via non-selective cleavages is two orders of magnitude higher than the A-factors characteristic of dissociation resulting from selective cleavages. This indicates that selective cleavages either are associated with substantial rearrangements or require a very specific conformation in order to undergo dissociation. The dynamics of specific fragmentation are very similar regardless of the nature of acidic residue and the position of the basic residue in the peptide sequence. However, peptides with C-terminal arginine display preferential cleavage at the acidic residue closest to arginine, while dissociation at both acidic residues with a slight preference to the residue remote from arginine is observed when arginine is moved to the N-terminus of a peptide.

Molecular mechanics modeling of the parent ion conformations shows extensive H-bonding within the three arginine-containing peptides. This is a direct result of the solvation of the protonated arginine residue by the peptide chain. Extensive interactions are observed between the basic arginine side chain and the

peptide bonds C-terminal to the aspartic and glutamic acid residues. This, in conjunction with H-bonding of the same peptide bond to the acidic side chains of the aspartic and glutamic acids, results in the preferential cleavages observed. Although the same acidic side chain interactions between aspartic and glutamic acids and the peptide bonds are observed in LDIFSDF, the absence of the highly basic arginine group results in many competing dissociation pathways for this peptide.

Acknowledgements

All of the work described herein was conducted at the W.R. Wiley Environmental Molecular Sciences Laboratory (EMSL), a national scientific user facility sponsored by the US Department of Energy and located at Pacific Northwest National Laboratory. PNNL is operated by Battelle for the US Department of Energy. Financial support for T.H.B was provided through NSF grant CHE-9634238. Research at EMSL was carried out within the project 40457 supported by the Office of Basic Energy Sciences of the US Department of Energy. The authors are gratefully thankful to Professors Bill Hase and Vicky Wysocki for very helpful discussions.

References

- [1] J.B. Fenn, M. Mann, C.K. Meng, S.F. Wong, C.M. Whitehouse, *Mass Spectrom. Rev.* 9 (1990) 37.
- [2] R.D. Smith, J.A. Loo, R.R.O. Loo, M. Busman, H.R. Udseth, *Mass Spectrom. Rev.* 10 (1991) 359.
- [3] A.L. McCormack, A. Somogyi, A.R. Dongre, V.H. Wysocki, *Anal. Chem.* 65 (1993) 2859.
- [4] A.R. Dongre, A. Somogyi, V.H. Wysocki, *J. Mass Spectrom.* 31 (1996) 339.
- [5] V. Grill, J. Shen, C. Evans, R.G. Cooks, *Rev. Sci. Instrum.* 72 (2001) 3149.
- [6] R.G. Cooks, T. Ast, A. Mabud, *Int. J. Mass Spectrom. Ion Process.* 100 (1990) 209.
- [7] J. Maaijer-Gielbert, J.H.M. Beijersbergen, P.G. Kistmaker, T.L. Weeding, *Int. J. Mass Spectrom. Ion Process.* 153 (1996) 119.
- [8] E.N. Nikolaev, A. Somogyi, D.L. Smith, C. Gu, V.H. Wysocki, C.D. Martin, G.L. Samuelson, *Int. J. Mass Spectrom.* 212 (2001) 535.

- [9] E. Stone, K.J. Gillig, B. Ruotolo, K. Fuhrer, A. Schultz, D.H. Russell, *Anal. Chem.* 73 (2001) 2233.
- [10] S. Mohammed, M.J. Chalmers, J. Gielbert, M. Ferro, L. Gora, D.C. Smith, S.J. Gaskell, *J. Mass Spectrom.* 36 (2001) 1260.
- [11] C. Lifshitz, *Mass Spectrom. Rev.* 1 (1982) 309.
- [12] P. Roepstroff, J. Fohlman, *J. Biomed. Mass Spectrom.* 11 (1984) 601.
- [13] R.S. Johnston, S.A. Martin, K. Biemann, *Int. J. Mass Spectrom.* 86 (1988) 137.
- [14] W. Yu, J.E. Vath, M.C. Huberty, S.A. Martin, *Anal. Chem.* 65 (1993) 3015.
- [15] J. Qin, B.T. Chait, *J. Am. Chem. Soc.* 117 (1995) 5411.
- [16] S.G. Summerfield, A. Whiting, S.J. Gaskell, *Int. J. Mass Spectrom. Ion Process.* 162 (1997) 149.
- [17] G. Tsapralis, H. Nair, A. Somogyi, V.H. Wysocki, W. Zhong, J.H. Futrell, S.G. Summerfield, S.J. Gaskell, *J. Am. Chem. Soc.* 121 (1999) 5142.
- [18] G. Tsapralis, A. Somogyi, E.N. Nikolaev, V.H. Wysocki, *Int. J. Mass Spectrom.* 195/196 (2000) 467.
- [19] S-W. Lee, H.S. Kim, J.L. Beauchamp, *J. Am. Chem. Soc.* 120 (1998) 3188.
- [20] A.G. Sullivan, F.L. Brancia, R. Tyldesley, R. Bateman, K. Sidhu, S.J. Hubbard, S.G. Oliver, S.J. Gaskell, *Int. J. Mass Spectrom.* 210/211 (2001) 665.
- [21] J. Laskin, M. Byrd, J.H. Futrell, *Int. J. Mass Spectrom.* 195/196 (2000) 285.
- [22] J. Laskin, J.H. Futrell, *J. Phys. Chem. A* 104 (2000) 5484.
- [23] J. Laskin, E. Denisov, J.H. Futrell, *J. Am. Chem. Soc.* 122 (2000) 9703.
- [24] J. Laskin, E. Denisov, J.H. Futrell, *Int. J. Mass Spectrom.* 219 (2002) 189.
- [25] S.A. Shaffer, K. Tang, G.A. Anderson, D.C. Prior, H.R. Udseth, R.D. Smith, *Rapid Commun. Mass Spectrom.* 11 (1997) 1813.
- [26] J. Laskin, E.V. Denisov, A.K. Shukla, S.E. Barlow, J.H. Futrell, *Anal. Chem.* 74 (2002) 3255.
- [27] M.W. Senko, J.D. Canterbury, S. Guan, A.G. Marshall, *Rapid Commun. Mass Spectrom.* 10 (1996) 1839.
- [28] P.J. Derrick, P.M. Loyd, J.R. Christie, in: I. Cornides, G. Howárth, K. Vékey (Eds.), *Advances in Mass Spectrometry*, vol. 13, Wiley, Chichester, 1995.
- [29] C. Gu, G. Tsapralis, L. Brecci, V.H. Wysocki, *Anal. Chem.* 72 (2000) 5804.
- [30] J. Laskin, J.H. Futrell, *J. Chem. Phys.* 116 (2002) 4302.